Predictive simulation of neutral beam injection on EAST in H- and L-mode plasma

2012 Phys. Scr. 85 035502

(http://iopscience.iop.org/1402-4896/85/3/035502)

Phys. Scr. **85** (2012) 035502 (5pp) doi:10.1088/0031-8949/85/03/035502

Predictive simulation of neutral beam injection on EAST in H- and L-mode plasma

Ji Wang[1,2], Chun-dong Hu[1,2], Bin Wu[2] and Jin-fang Wang[2]

[1] University of Science and Technology of China, Hefei 230026, People's Republic of China
[2] Institute of Plasma Physics, China Academy of Sciences, Hefei 230031, People's Republic of China

E-mail: wangji@ipp.ac.cn

Received 20 October 2011
Accepted for publication 13 January 2012
Published 7 February 2012
Online at stacks.iop.org/PhysScr/85/035502

Abstract
The Experimental Advanced Superconducting Tokamak (EAST) simulations are carried out for neutral beam injection (NBI) in L- and H-mode plasma using the transport code ONETWO and the Monte Carlo code NUBEAM. The results predicted with different beam energy injections are presented and analyzed. The heating efficiency, shine-through power loss, current drive, beam ion trapping fraction and neutron emission with respect to different beam energy and discharge modes are discussed and some guidelines are provided for future experiments with NBI on EAST.

PACS numbers: 52.50.Gj, 52.65.−y

1. Introduction

The Experimental Advanced Superconducting Tokamak (EAST) tokamak is a fully superconducting fusion device and one of its missions is to explore and demonstrate long-duration discharge (1000 s) maintained by non-inductive current drive. Auxiliary heating is needed for EAST to get the experimental physical parameters. The neutral beam injection (NBI) system, an important means of auxiliary heating and current drive for EAST, is under construction. The NBI system of EAST has been designed with co-injection and counter-injection. The first two neutral beam ion sources have been designed and are currently being constructed for co-injection on window A, and the next two sources will be constructed for counter-injection on window F in the next stage, as shown in figure 1.

The angle between the two beams on the same window is 8.7°. The best co-injection scenario direction angle is 19.5° between the bisector of the two beams and the vertical of window A [1, 2].

Some perfect physical results have been achieved on EAST and the high confinement mode (H-mode) has successfully been achieved in a winter experiment in 2010. Predictive simulation and data analysis are rather valuable and important for scientists to guide future work. Some simulations were carried out to predict the results due to NBI from different parameter aspects [1, 3, 4]. In this paper, we use ONETWO and NUBEAM codes to simulate NBI in L- and H-mode discharges on EAST. The neutral beam simulation code NUBEAM has been successfully integrated into the transport code ONETWO[3]. The NUBEAM module is a Monte Carlo package for time-dependent modeling of fast ion species in an axisymmetric tokamak. The NUBEAM module includes the physics of neutral beam deposition, fast ion two-dimensional (2D) orbiting, power deposition, beam-driven current and transfer accounting for particle collisions, charge exchange loss and recapture, and transport of beam particles [5]. The ONETWO transport code solves the flux surface averaged transport equation for energy, particles, toroidal rotation, current density and equilibrium evolution with self-consistent source and sink calculation [6, 7]. The ONETWO has been widely applied and the NUBEAM has been extensively validated against data from the PLT, PDX, PBX, TFTR, DIII-D, ASDEX, JET, JT-60 and TEXTOR tokamaks[4].

The two tangential co-injection beams are only included in this predictive simulation. In section 2 we present two different L- and H-mode scenarios applying the Weiland anomalous transport model with variational beam energy, while the plasma density and beam power are fixed in time. In section 3 numerical results of the two scenarios are presented.

[3] https://fusion.gat.com/THEORY/onetwo/
[4] http://w3.pppl.gov/ntcc/NUBEAM

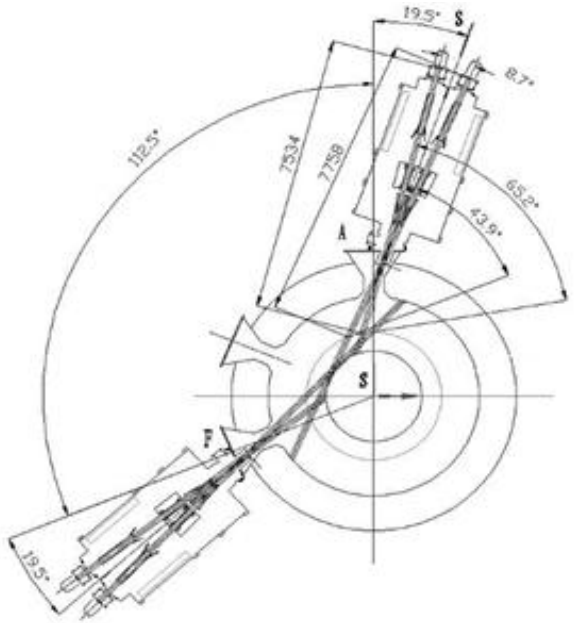

Figure 1. Schematic diagram of NBI of EAST.

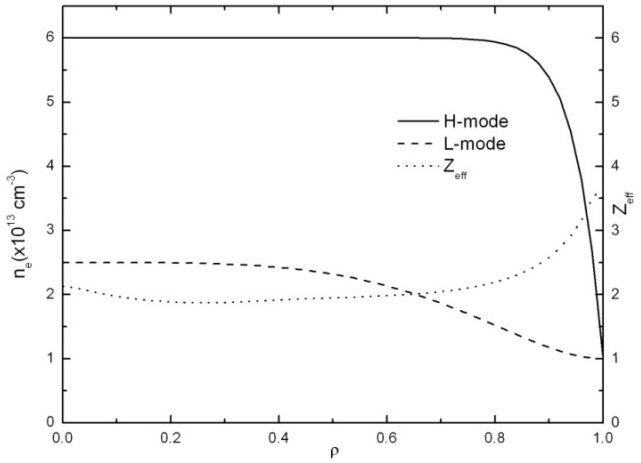

Figure 2. The constant n_e and Z_{eff} profiles in the evolution process of plasma.

Finally, a summary and the plan for future work are presented in section 4.

2. Different discharge mode scenarios

In this section, two different plasma confinement modes (L- and H-mode) with low density and high density, respectively, are considered. The density of the two modes and the Z_{eff} distribution are constant as shown in figure 2. The impurity is assumed to be carbon. ρ is defined as $\rho = \sqrt{\Phi/\pi B_t}$, where Φ is the toroidal magnetic flux inside a given flux surface. The electron temperature T_e and ion temperature T_i profiles of the target plasma are assumed to be the same with $T_e(0) = T_i(0) = 1.2$ keV. The magnetic equilibrium configuration is calculated from the EFIT code with toroidal current $I = 1$ MA, $B_t = 3.0$ T, $R = 1.75$ m and $a = 0.4$ m as shown in figure 3.

In order to study the beam injection efficiency in L- and H-mode plasma with variational energy and fixed power on EAST, the beam power is preferred to be 4 MW and the energy is selected among 60, 70 and 80 keV. The major NBI parameters of EAST are listed in table 1. The plasma discharge duration with NBI is 1.5 s. The beam power and energy over the discharge duration remain steady and constant.

Table 1. The major NBI parameters of EAST in the simulation.

	Beam_1	Beam_2
Beam energy	60, 70 and 80 keV	60, 70 and 80 keV
Beam power	2 MW	2 MW
Injection direction	Co-current	Co-current
Aperture shape	Rectangular	Rectangular
Tangency major radius	73.4047 cm	126.1253 cm
Horizontal divergence	0.6°	0.6°
Vertical divergence	1.2°	1.2°
$E : E_{1/2} : E_{1/3}$	80%:14%:6%	80%:14%:6%

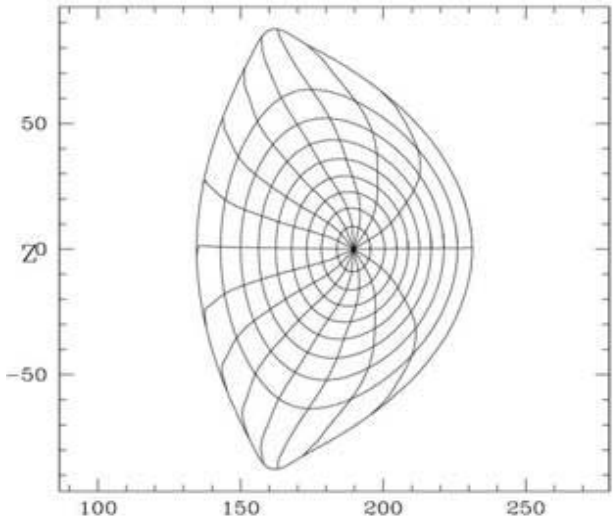

Figure 3. Equilibrium configurations (cm).

3. Numerical results

NBI heated discharge is modeled self-consistently in the evolution of the plasma equilibrium configuration with a fixed boundary as shown in figure 3. One of the differences between the L- and H-modes is that the H-mode exists in an edge transport barrier, i.e. the so-called pedestal shown in figure 2. In the simulation, a nonlinear calculation solver is involved to get self-consistent numerical solution. The Weiland model derived by linearizing the fluid equations with magnetic drifts for each plasma species is applied in the transport code ONETWO to compute the transport due to ion temperature gradient (ITG), the trapped electron mode (TEM), including electromagnetic effects, as well as the effects of electron–ion collisions, impurities and fast ions [8].

3.1. Heating efficiency

The temperatures of the two discharge modes evolved with NBI after 1.5 s are shown in figures 4 and 5. It can be seen that the electron and ion temperatures have been greatly improved in both the L- and H-modes. An outstanding feature is that there is a separatrix where electrons and ions have the same

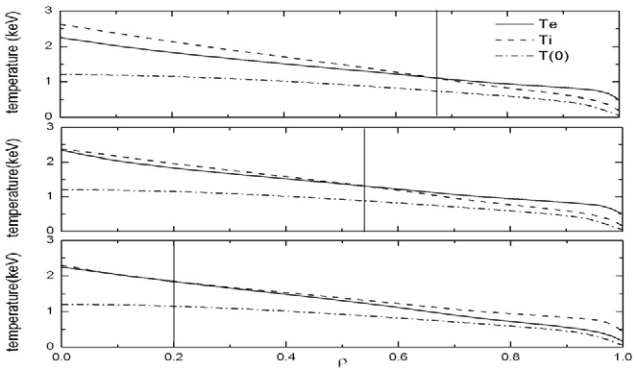

Figure 4. L-mode temperature profile at $t = 1.5$ s.

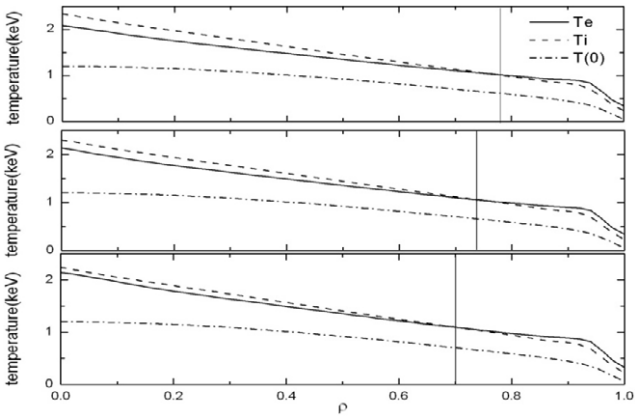

Figure 5. H-mode temperature profile at $t = 1.5$ s.

temperature. In fact, the separatrix corresponds to a certain flux surface. The temperature of ions is higher than that of electrons inside the surface, whereas the electron temperature is higher outside the surface. In particular, the distance between the surfaces and magnetic axis in low density is much shorter than that in high density, and the distance in the same density is also shorter with increasing beam energy. The neutral beam injection produces fast ions that carry high kinetic energy. At high injection velocity, the electron heating is initially dominant, and as the beam ions slow down, the heating is transferred to the ions [9].

In the case of low density, the slowing down path of fast ions is relatively longer, and when the beam energy is higher, the path is even much longer. With an increase of beam energy, the zone where the electron heating is dominant is then broader. After NBI for 1.5 s, the core temperature profile tends to be peaked in both the L- and H-modes. Although the total number of particles in the L-mode is much less than that in the H-mode, the general resulting heating profiles between them are closer because a large part of the beam energy in the L-mode shines through as shown in figure 7.

3.2. Current drive

The profiles of beam-driven current density are shown in figure 6.

The beam-driven current density in low density of the L-mode is obviously higher than that in high density of the H-mode inside $\rho = 0.9$ and the difference between the currents due to beam energies 70 and 80 keV is not very

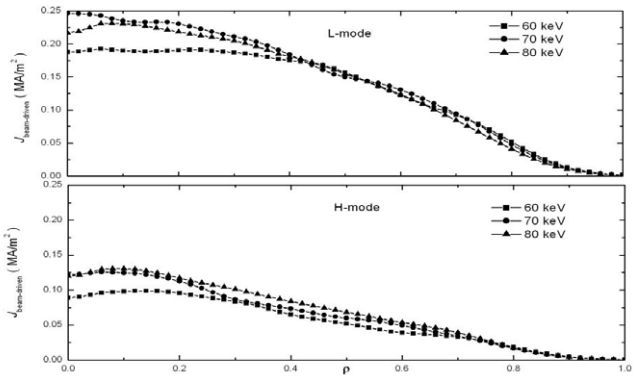

Figure 6. Beam-driven current density profiles at $t = 1.5$ s.

significant. This means that the beam-driven current density tends to saturate with a beam energy increase. This can be explained as follows.

As far as the effects of trapped and untrapped electrons on beam-driven current are concerned, the modified beam-driven density expression [10] is

$$J_{\text{beam-driven}} = J_f \left[1 - \frac{Z_{\text{b}}}{Z_{\text{eff}}}(1 - G)\right], \tag{1}$$

where

$$J_f = (eZ_b S\tau_{se} V_b)\xi_0 x_b J_0 F_{nc}. \tag{2}$$

The factor G has some different expressions, and one of them [11] is

$$G = (1.55 + 0.85/Z_{\text{eff}})\varepsilon^{1/2} - (0.2 + 1.55/Z_{\text{eff}})\varepsilon, \tag{3}$$

$$\tau_{\text{se}} = 3m_{\text{e}}v_{\text{e}}^3 m_{\text{f}}/\left(16\sqrt{\pi}e^4 Z_f^2 n_{\text{e}} \ln\Lambda\right)$$
$$\approx 1.17 \times 10^{18} A_{\text{b}}(T_{\text{e}}/KeV)^{3/2}/Z_{\text{b}}^2 n_{\text{e}} \propto \frac{T_{\text{e}}^{3/2}}{n_{\text{e}}}. \tag{4}$$

According to (4), we can conclude that $J_{\text{beam-driven}} \propto T_{\text{e}}^{3/2}/n_{\text{e}}$. In the case when the density is fixed in time, we can obtain $J_{\text{beam-driven}} \propto T_{\text{e}}^{3/2}$ at different times. T_{e} will finally reach a saturated state because with an increase of neutral beam energy, the beam power loss tends to increase, and the power deposition contributions above a certain threshold to heat target electrons tend to almost saturate. The T_{e} will gradually tend to become stable and the $J_{\text{beam-driven}}$ will also tend to saturate with the neutral beam long duration injection.

3.3. Shine-through power loss

The beam neutrals not ionized by Coulomb collision with the target electrons and ions can shine through the plasma, and a part of the beam power is lost. The shine-through power loss is presented in figure 7. It demonstrates that the shine-through power loss in low density of L-mode is much higher than that in high density of H-mode. With an increase of beam energy the power loss gradually tends to increase in the same mode. From the results we must avoid the case when a high-power and energetic neutral beam is injected in low density and the neutral beam damages the vacuum chamber wall, and at the same time some appropriate measures should be taken in the local area where the neutral beam may hit. For this

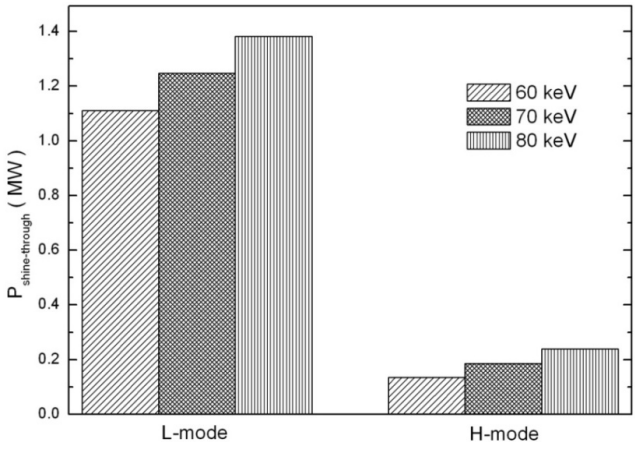

Figure 7. Shine-through power loss at $t = 1.5$ s.

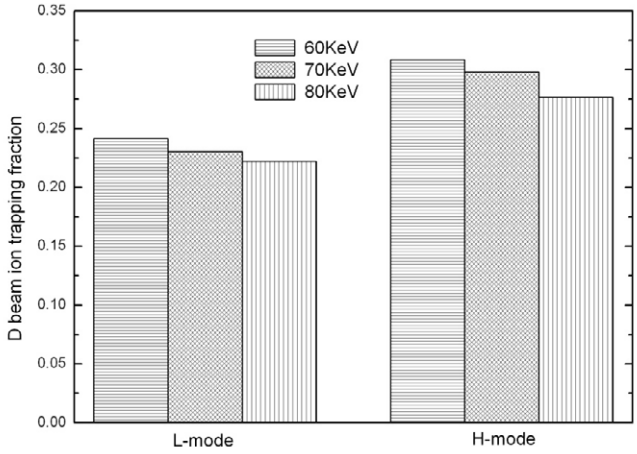

Figure 8. Beam ion trapping fraction.

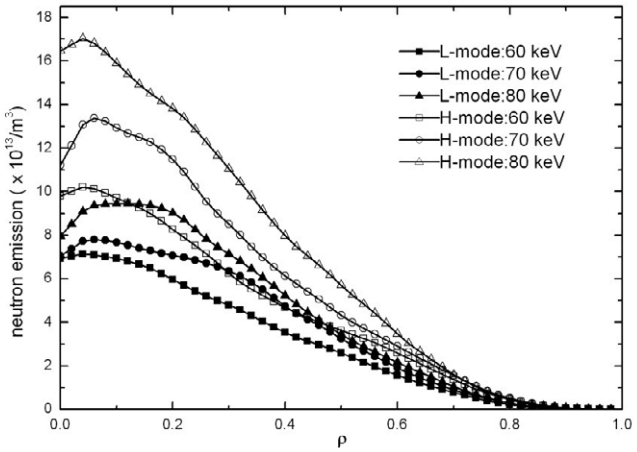

Figure 9. Beam-target neutron emission density profiles at $t = 1.5$ s.

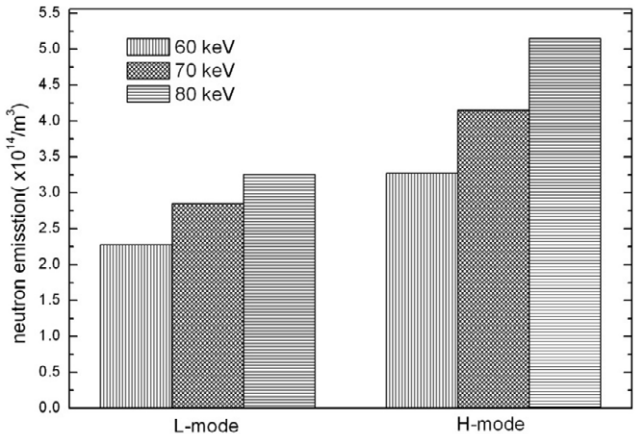

Figure 10. Integrated values of beam-target neutron emission density profiles at $t = 1.5$ s.

purpose, further predictive simulations need to calculate the maximum shine-through power deposition on the wall with the conditions of current or future experimental physical parameters on EAST and to use optimal materials according to the power deposition intensity.

3.4. Beam ion trapping fraction

The beam atoms become ionized through Coulomb collisions by charge exchange and ionization. The deuterium beam ion trapping fraction is illustrated in figure 8. It indicates that the beam ion trapping fraction in L-mode is lower than that in H-mode, and with an increase of the beam energy, the trapping fraction decreases gradually. Qualitatively, the charge exchange cross-section σ_{ch}, the ion ionization cross-section σ_i and the electron ionization cross-section σ_e in high density are larger than those in low density. The larger the collision cross-section, the greater the ion-trapping fraction. According to Wesson's view, in the same plasma mode, σ_{ch} and σ_e will increase when the beam atom energy decreases from 80 to 60 keV [9]. It is not necessary to maximize the beam energy to obtain the ideal beam ion trapping fraction.

3.5. Neutron emission

Neutrons are the fusion products and also the reactants during the fusion reaction. In these simulations, the neutron emission density of the beam-target reaction in the L-mode is lower than that in the H-mode at the same energy as shown in figures 9 and 10. It also indicates that the larger the injected energy, the greater the number of neutrons generated in the same mode. In these simulations, neutrons are the products of the reaction between deuteron and deuteron. With an increase of the deuterium beam energy, the deuteron–deuteron reaction cross-section increases [9]. The increasing reaction section results in greater neutron emission. The difference between the neutron densities is not so large outside $\rho = 0.8$ in both L- and H-modes. This means that the plasma edge effects on the beam-target neutron emission are not very strong in these two modes.

4. Summary

In these simulations, we applied the transport code ONETWO and the beam Monte Carlo code NUBEAM with different L- and H-modes to predict the results of co-injection NBI on EAST. The Weiland anomalous transport model with different beam energies is applied to compute self-consistently the temperature, shine-through power loss, current drive, beam ion trapping fraction and neutron emission. The main predictions of NBI on EAST can be described as follows.

(i) The EAST temperature in L- and H-modes obviously increases after the NBI. There is a dividing flux surface and the ion temperature is higher than electron temperature inside the surface. The distance between the surfaces and the magnetic axis in both H- and L-mode tends to decrease with increasing beam energy. The core temperature profile tends to be peaked in both L- and H-mode discharge.

(ii) The beam-driven current density in the L-mode is obviously higher than that in the H-mode inside $\rho = 0.9$ and the difference of beam-driven currents due to beam energies 70 and 80 keV is not very significant. This means that in the case of the specified beam injection power, just improving the beam energy in order to drive a higher current is not feasible when the beam energy exceeds a certain threshold.

(iii) The shine-through power loss in the L-mode is much higher than that in the H-mode, and with an increase of beam energy, the power loss tends to gradually increase in the same mode. Appropriate protective measures should be adopted to avoid the damages caused by the beam hit.

(iv) The beam ion trapping fraction in the L-mode is obviously lower than that in the H-mode and with an increase of the beam energy, the trapping fraction decreases gradually.
Properly reducing the beam energy can increase the beam ion trapping fraction.

(v) The larger the injected energy, the greater the number of neutrons generated in both L- and H-modes. The neutron emission density of beam-target reaction in the L-mode is lower than that in the H-mode with the same beam energy. The difference of neutron emission density in these two modes is not too significant outside $\rho = 0.8$ in the two modes.

Complicated simulations of NBI located on window A for co-injection and window F for counter-injection and some mixed auxiliary heating will be conducted in the next stage.

Acknowledgments

We thank Dr Lei Ye and Qilong Ren for their help in using ONETWO and NUBEAM. We also thank the National Transport Code Collaboration (NTCC) and General Atoms (GA) for their contribution to the development of fusion codes. This work was supported by the National Natural Science Foundation of China (grant numbers 10975160 and 11175211).

References

[1] Wang J F, Wu B and Hu C D 2010 *Plasma Sci. Technol.* **12** 289–94
[2] Wu B *et al* 2011 *Fusion Eng. Des.* **86** 947–50
[3] Zhou D *et al* 2009 *Plasma Sci. Technol.* **11** 417–21
[4] Ni Q L *et al* 2010 *Plasma Sci. Technol.* **12** 661–7
[5] Pankin A *et al* 2004 *Comput. Phys. Commun.* **159** 157–84
[6] Kessel C E *et al* 2007 *Nucl. Fusion* **47** 1274–84
[7] Murakami M *et al* 2005 *Nucl. Fusion* **45** 1419–26
[8] Bateman G *et al* 1998 *Phys. Plasmas* **5** 1793–9
[9] Wesson J 2003 *Tokamaks* (Oxford: Clarendon)
[10] Okano K 1990 *Nucl. Fusion* **30** 423–30
[11] Mikkelsen D R and Singer C E 1983 *Nucl. Technol. Fusion* **4** 237–52